Electronic Supplementary Material (ESI) for Physical Chemistry Chemical Physics.
This journal is © the Owner Societies 2016

Electronic Supplementary Information

Rational Design of Hierarchical ZnO Superstructures for Efficient Charge Transfer: Mechanistic and Photovoltaic Studies of Hollow, Mesoporous, Cage-Like Nanostructures with Compacted 1D Building Blocks

Tridip Ranjan Chetia,[a] Mohammad Shaad Ansari[a] and Mohammad Qureshi[a*]

[a]Materials Science Laboratory, Department of Chemistry, Indian Institute of Technology Guwahati, Assam, 781039, India.

*E-mail: mq@iitg.ernet.in, Tel: +91-361-2582320, Fax: +91-361-2582349.

1. PXRD pattern of the synthesized ZnO heterostructures:

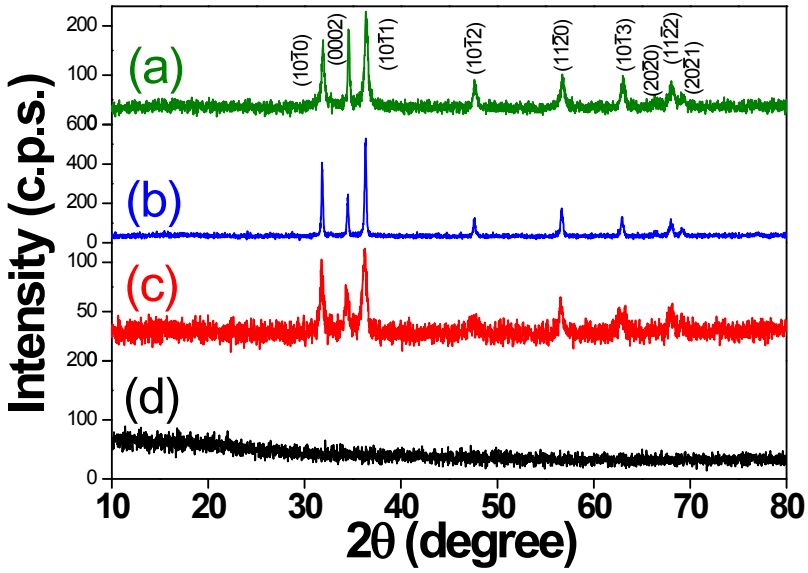

Figure S1. PXRD patterns for (a) ZnO cages, (b) ZnO nanorods (c) porous ZnO nanoparticles obtained after calcination of amorphous product (d).

2. Crystallite size calculations

The estimated the crystallite sizes of ZnO Cage, ZnO NRs and ZnO PNPs are calculated by using Debye-Scherrer equation are shown in table S1. The Scherrer equation is represented as:

$$D = \frac{0.95 \times \lambda}{\Delta W \times \cos\theta}$$

Where, D is the crystallite domain diameter, λ is the wavelength of the incident X-ray beam (1.54 Å for the Cu Kα), θ is the Bragg's diffraction angle, ΔW the width of the X-ray pattern line at half peak-height in radians.

Table S1. Calculated crystallite size obtained from figure S1 of the ZnO heterostructures by using Debye-Scherrer equation along with intensity in counts per second (c.p.s) for highest intense peak are:

Name of the compound	FWHM	Crystallite size D (nm)	Intensity maximum (c.p.s.)	2θ (degree)	Crystal plane
ZnO Cages	0.46	25.7	215.4	36.4	$(10\bar{1}1)$
ZnO NRs	0.23	41.9	503.3	36.3	$(10\bar{1}1)$
ZnO PNPs	0.57	15.3	112.5	36.2	$(10\bar{1}1)$

From table S1 we have seen that the average crystallite size and peak intensity for the highest intense peak is maximum for ZnO NRs synthesized in the control reaction in presence of only NH_4OH. These observations are suggestive of higher crystal quality of ZnO NRs than the other two samples ZnO Cages and ZnO PNPs.

3. PXRD pattern of vertically grown ZnO NRs, ZnO NR assembled superstructures and bare ZnO NRs laying parallel to the substrate:

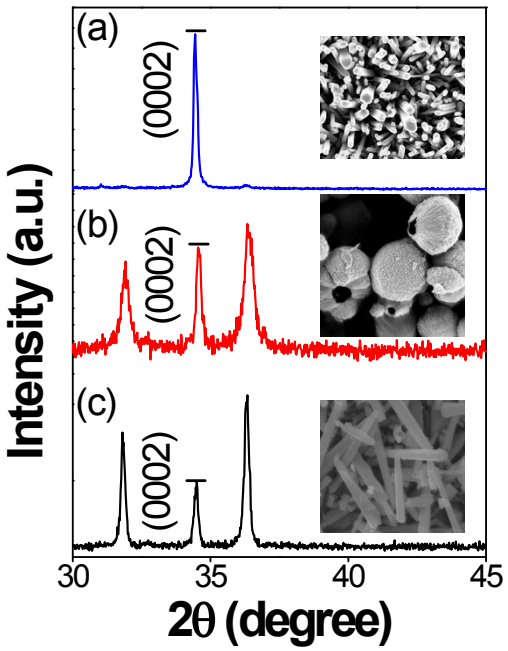

Figure S2. XRD patterns showing variation of appearance for the peak (0002) obtained for (a) vertically grown ZnO NRs on the substrate (b) ZnO cages and (c) ZnO NRs laying horizontally on the substrate.

4. PXRD patterns of the products obtained by different addition amount of NH_4OH

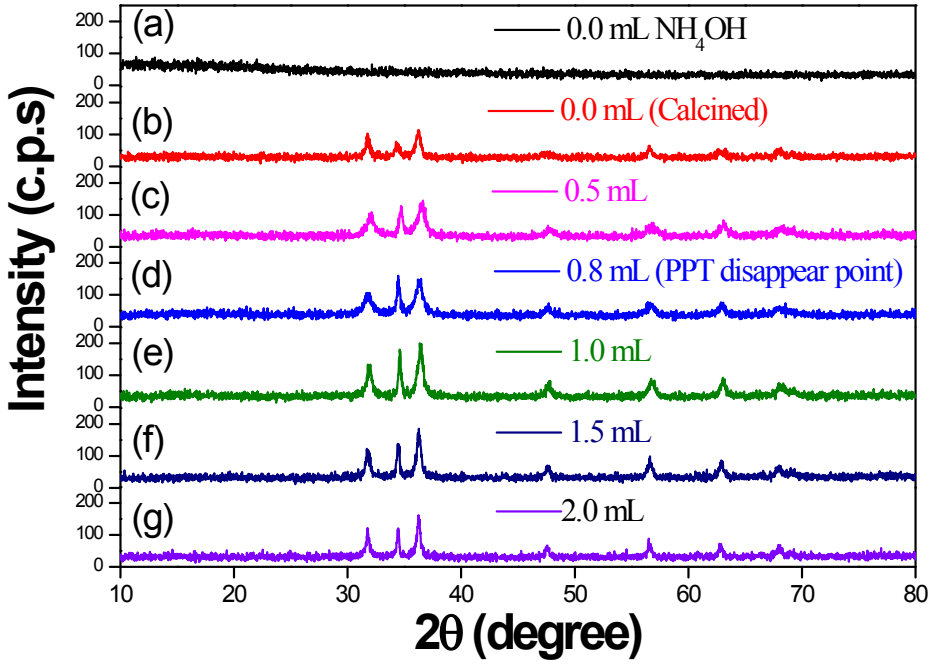

Figure S3. PXRD patterns obtained for different addition amount of NH_4OH, i.e. (a) amorphous product obtained in absence of NH_4OH, (b) calcined product of (a), (c) 0.05 mL, (d) 0.08 mL, (e) 1.0 mL, (f) 1.5 mL and (g) 2.0 mL.

Table S2: Calculated crystallite size and intensity in counts per second (c.p.s) of the highest intense peak obtained from the PXRD patterns of figure **S3**.

Name of the compound	FWHM	Crystallite size D (nm)	Intensity maximum (c.p.s)	2θ (degree)	Crystal plane
ZnO_0.0 mL	0.57	15.3	112.5	36.3	$(10\bar{1}1)$
ZnO_0.5 mL	0.92	12.9	137.0	36.5	$(10\bar{1}1)$
ZnO_0.8 mL	0.39	13.3	144.6	34.5	(0002)
ZnO_1.0 mL	0.65	19.3	184.2	36.5	$(10\bar{1}1)$
ZnO_1.5 mL	0.46	25.7	215.4	36.4	$(10\bar{1}1)$
ZnO_2.0 mL	0.19	28.3	148.9	36.3	$(10\bar{1}1)$

From table S2 it is pragmatic that crystallite size and intensity of the highest intense peak in the PXRD patterns varies significantly with the addition amount of NH_4OH in the reaction. Hence the crystallinity of the synthesized ZnO depends on the concentration of NH_4OH. Highest value of crystallite size (~28.3 nm) is observed in case of ZnO perceived in the reaction with 2.0 mL of NH_4OH. However, the intensity maximum is highest for the product obtained in the reaction with 1.5 mL of NH_4OH and also the crystallite size (~25.7 nm) is comparable with the former one.

5. Low magnification FESEM images of the products obtained by different addition amount of NH_4OH

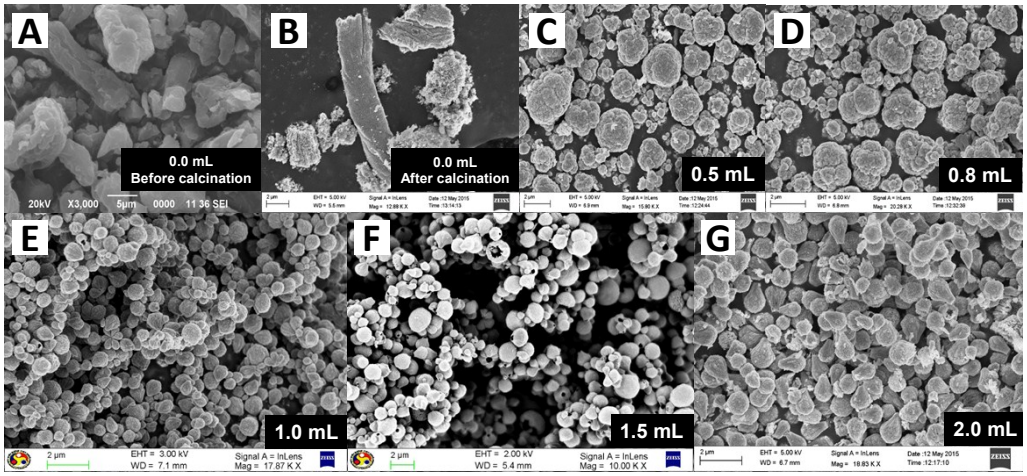

Figure S4. Low magnification FESEM images of the products obtained from the reactions with (A) 0.0 mL NH_4OH before calcination, (B) calcined product of (A), (C) 0.05 mL NH_4OH, (D) 0.8 mL NH_4OH, (E) 1.0 mL NH_4OH, (F) 1.5 mL NH_4OH and (G) 2.0 mL NH_4OH.

6. TEM analysis of the ZnO NPs obtained by ultra-sonication of ZnO PNPs synthesized in the reaction 3.

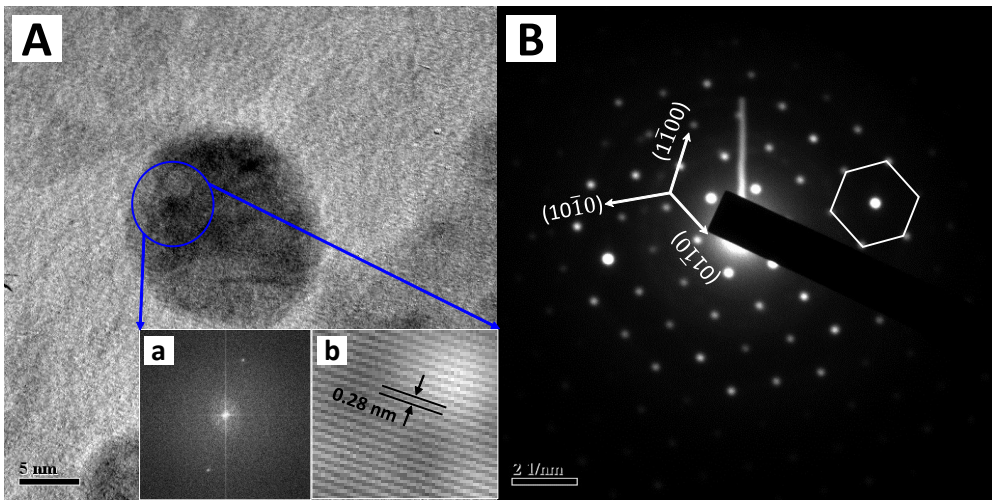

Figure S5. TEM image (A) represents a ZnO nanoparticle obtained from ZnO PNPs after ultra-sonication and image (B) is the corresponding SAED pattern. Insets (a) and (b) to figure (A) portrays FFT and IFFT showing interplanar spacing of the crystal planes.

TEM image (A) displays a single ZnO nanoparticle (NP) obtained from the porous ZnO NPs after ultra-sonication. The size of the particles are in the range of ~10–15 nm and each particle is

diffracting as a wurtzite single crystal as evident from the selected area electron diffraction (SAED) pattern. The SAED pattern is appear to be hexagonally symmetrical and is indexed as [0001] zone axis which is recognized as most favorable crystal growth direction of ZnO. The Fast Fourier transform (FFT) pattern [inset (a) to image (A)] is accord with the diffraction pattern of the [0001] zone axis of ZnO and the interplanar spacing of the lattice pattern is found to be ~0.28 nm which corresponds to the $(10\bar{1}0)$ lattice planes. This observation suggests inhibited growth of the ZnO NPs along (0001) direction and favorable growth along six symmetric directions of $\pm(10\bar{1}0)$, $\pm(1\bar{1}00)$, and $\pm(0\bar{1}10)$ lattice planes.

7. TEM, SAED and IFFT features of the ZnO NRs synthesized in presence of NH_4OH only

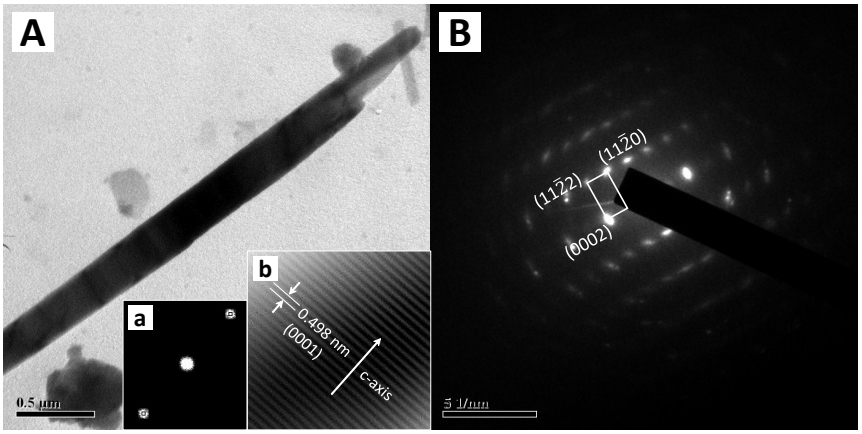

Figure S6. TEM image (A) represents a single ZnO nanorod obtained from the reaction carried out in presence of NH_4OH only and image (B) is the corresponding SAED pattern. Insets (a) and (b) to figure (A) portrays FFT and IFFT showing interplanar spacing of the crystal planes.

TEM image (A) shows a single ZnO NR obtained from the control reaction carried out in presence of only NH4OH. The diameter of the ZnO NR is found to be ~200 nm while the longitudinal dimension is ~2–3 μm. The corresponding SAED pattern in image (B) reveals the wurtzite single crystalline structure of the NRs and indexed as $(1\bar{1}00)$ zone axis which is in good agreement with the FFT pattern shown in the inset (a) to image (A). The crystal growth anisotropy of the ZnO NRs along (0001) direction or the c-axis is unfolded in the IFFT pattern shown in the inset (b) to image (A) in which the lattice spacing is found to be ~0.50 nm corresponds to the (0001) crystal planes.

8. Low Magnification FESEM images of the products obtained by varying addition amount of sodium alginate (ALG)

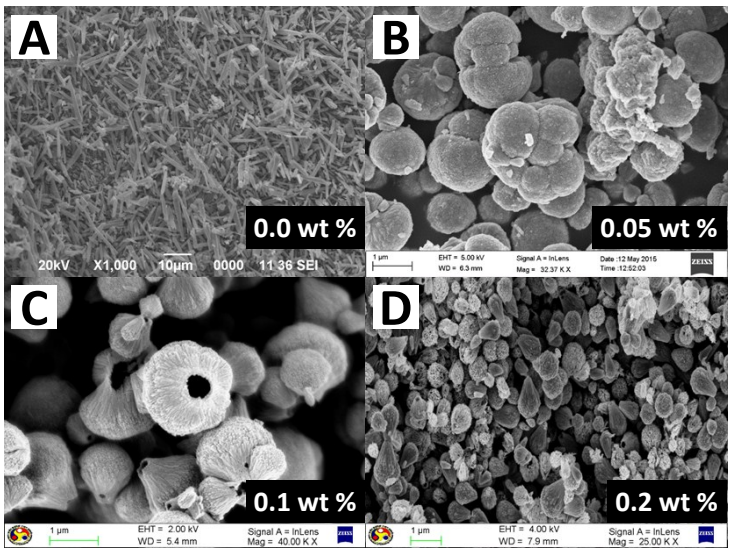

Figure S7. Low magnification FESEM images of products obtained during optimization of addition amount of ALG (A) ZnO NRs from the control reaction, (B) Irregular larger size ZnO cages in presence of 0.05 wt % ALG, (C) anticipated ZnO cages in presence of 0.1 wt % ALG and (D) smaller size along with some partially formed ZnO cages in presence of 0.2 wt % ALG.

9. PXRD patterns of the products obtained by different addition amount of sodium alginate (ALG)

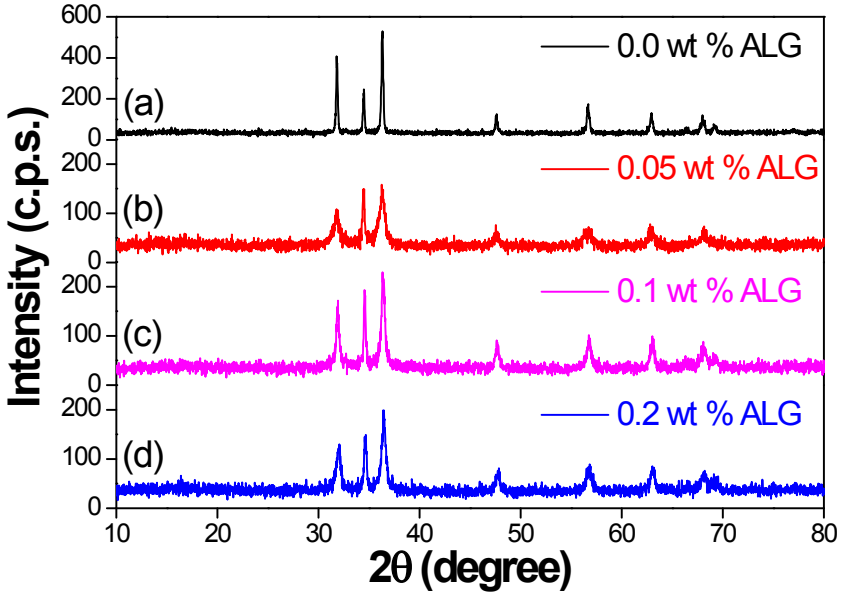

Figure S8. PXRD patterns obtained for the ZnO synthesized with different addition amount of sodium alginate (ALG) in weight percent, i.e. (a) in absence of ALG, (b) 0.05 wt % ALG, (c) 0.1 wt % ALG and (d) 0.2 wt % ALG.

Table S3. Calculated crystallite size and intensity in counts per second (c.p.s) of the highest intense peak obtained from the PXRD patterns of figure S8

Name of the compound	FWHM	Crystallite size (nm)	Intensity maximum (c.p.s)	2θ (degree)	Crystal plane
ZnO _0.0 wt % ALG	0.23	41.9	503.3	36.302	$(10\bar{1}1)$
ZnO_0.05 wt % ALG	0.35	20.9	145.0	36.280	$(10\bar{1}1)$
ZnO_0.1 wt % ALG	0.46	25.7	215.4	36.409	$(10\bar{1}1)$
ZnO_0.2 wt % ALG	0.56	19.3	196.4	36.445	$(10\bar{1}1)$

From table S3, amongst all the synthesized products, the crystallite size and intensity maximum are highest for the ZnO NRs obtained in the control reaction indicating its high crystallinity. However, the crystallinity of the product obtained in the reactions in presence of 0.1 wt % ALG is highest amongst the ZnO synthesized in presence of 0.05 wt % ALG and 0.2 wt % ALG. The variation of crystallinity of the ZnO superstructures with respect to the addition amount of ALG demonstrates the effect of it in the crystal growth habits of ZnO.

10. PXRD patterns of the products obtained different time interval

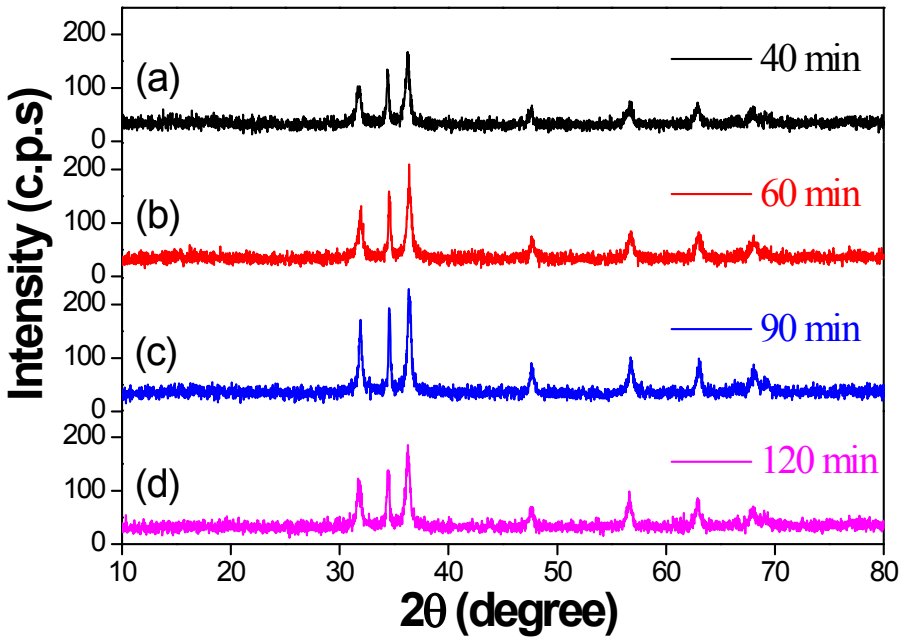

Figure S9. PXRD patterns obtained for the synthesized ZnO by varying reaction time, i.e. (a) 40 min, (b) 60 min, (c) 90 min and (d) 120 min.

Table S4. Calculated crystallite size and intensity in counts per second (c.p.s) of the highest intense peak obtained from the PXRD patterns of figure S9

Name of the compound	FWHM	Crystallite size D_p (nm)	Intensity maximum (c.p.s.)	2θ value (degree)	Crystal plane
ZnO_40 min	0.57	20.0	165.6	36.2	$(10\bar{1}1)$
ZnO_60 min	0.55	21.0	192.2	36.4	$(10\bar{1}1)$
ZnO_90 min	0.46	25.7	215.4	36.4	$(10\bar{1}1)$
ZnO_120 min	0.52	19.5	181.4	36.3	$(10\bar{1}1)$

From table S4 it is clear that high quality ZnO superstructures are synthesized in case of the reaction time of 90 min for which higher crystallite size as well as higher intensity PXRD peak for $(10\bar{1}1)$ crystal plane are observed. Further increase in reaction time leads to decrease in crystallinity of the product which is due to dissolution of ZnO as evident from the FESEM analysis.

11. Low magnification FESEM topographies of the products obtained at reaction time (A) 40 min and (B) 120 min

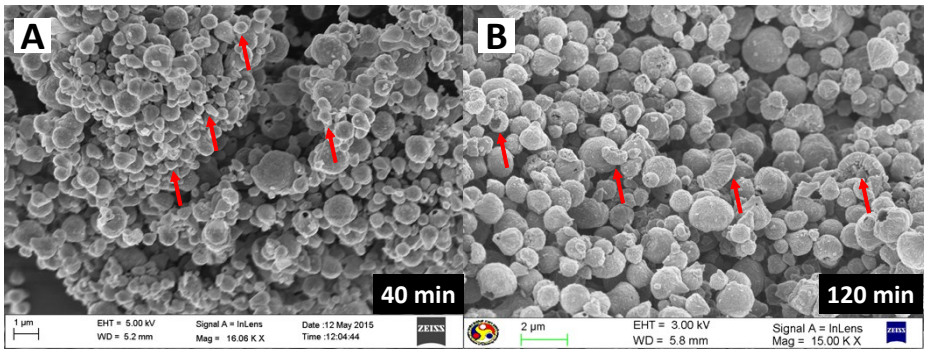

Figure S10. Low magnification FESEM images of the ZnO superstructures obtained at (A) 40 min and (B) 120 min of reaction time.

Figure S10 (A) and (B) represents low magnification FESEM features of ZnO obtained at 40 min and 90 min of reaction time respectively. Red arrows in image (A), indicates highly populated partially developed smaller cages which are observed due to insufficient reaction time (40 min) while in image (B) designates broken ZnO superstructures caused by excess reaction time (120 min).

12. Fourier transform infrared (FTIR) spectroscopy analyses of [Zn^{2+}–ALGI] complex

We have probed the formation of a complex between alginate ions (ALGI) and Zn^{2+} ions, i.e., [Zn^{2+}–ALGI]; by performing FTIR analysis for the gelatinous precipitate extracted from the reaction mixture.

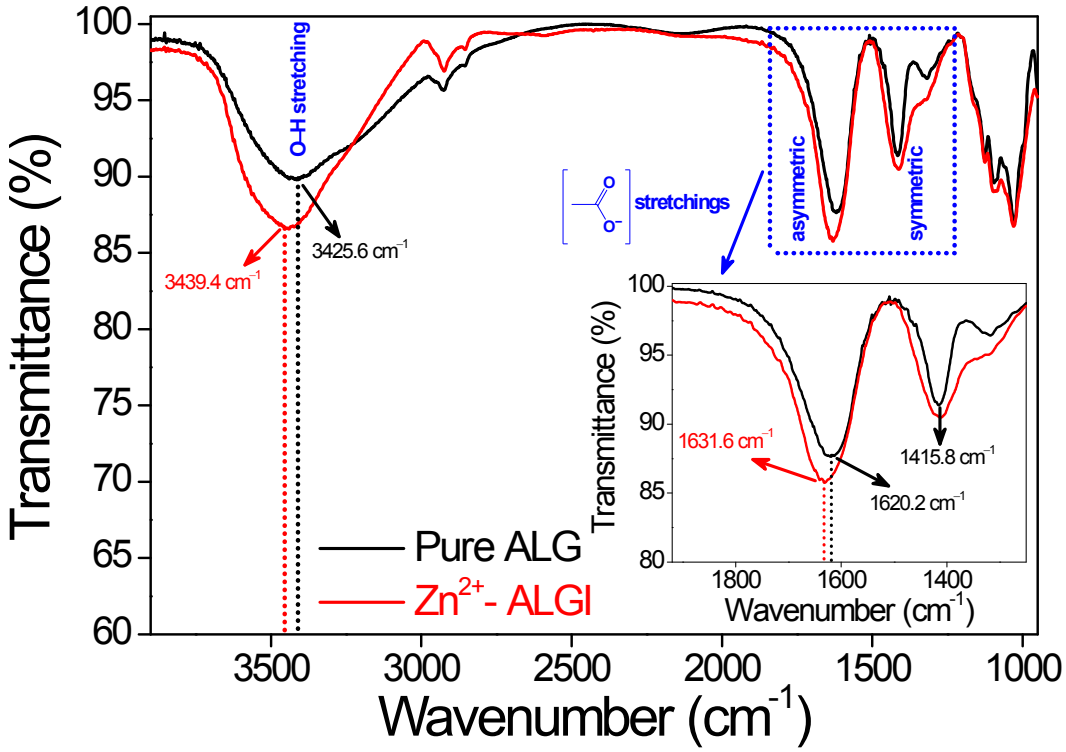

Figure S11. FTIR spectra for pure sodium alginate (ALG), [black line] and for the complex [Zn^{2+}–ALGI] extracted from the reaction mixture (red line). Inset to it shows the enlarged view of the shifting of stretching bands for carboxylate groups in the [Zn^{2+}–ALGI] complex compared to the pure ALG.

Figure S11 represents the FTIR spectra recorded for pure sodium alginate (ALG), [black line] and the gelatinous precipitate appeared immediately after the addition of $Zn(NO_3)_2.6H_2O$ to the aqueous solution of ALG (red line). It is observed that, the broad absorption band around 3425.6 cm^{-1} for pure ALG which is due to the stretching of hydroxyl (–OH) groups[1] is shifted toward higher wavenumber, i.e., 3439.4 cm^{-1} after adsorption of Zn^{2+} ions from the solution. Moreover, the asymmetric stretching band (~1620 cm^{-1}) for the carboxylate groups ($–COO^-$) in ALG[1] is also shifted toward higher wavenumber value, i.e., 1631.6 cm^{-1}. Observed shifting of vibrational bands for the (–OH) and ($–COO^-$) groups in ALG after the addition of Zn^{2+} ions are indicating the coordination of metal ions to the functional groups which leads to the formation of complex [Zn^{2+}–ALGI].

13. Steady-State Photoluminescence study of the photoanodes after calcination

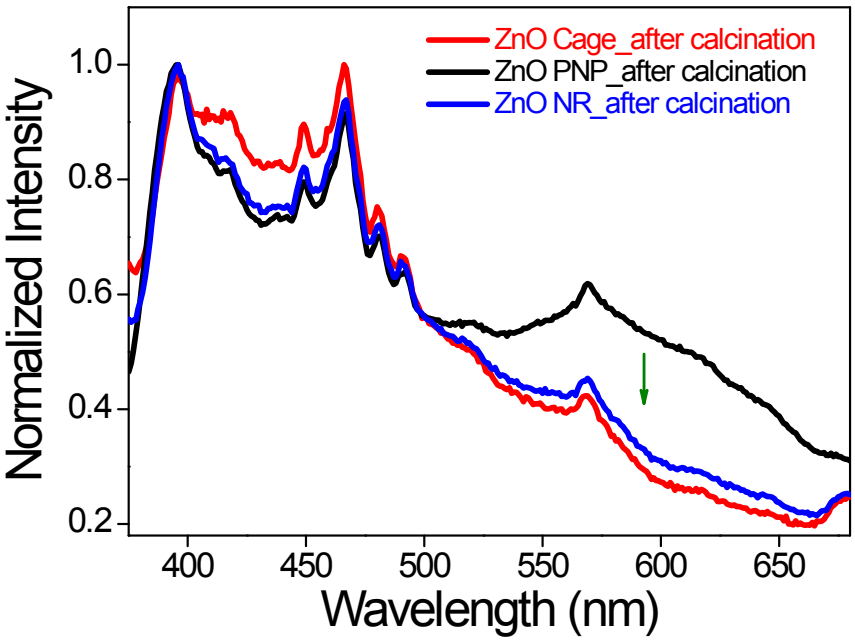

Figure S12. Steady-State Photoluminescence Spectra for the photoanodic films on FTO substrates namely ZnO cage (red line), ZnO PNP (black line), and ZnO NR (blue line) recorded at an excitation wavelength of 355 nm.

14. Steady-State Photoluminescence study of the dye sensitized photoanodes

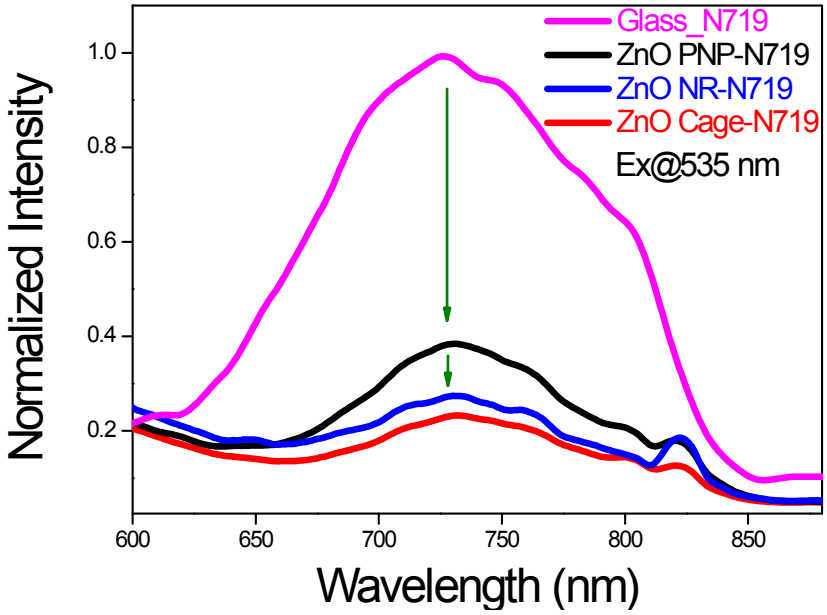

Figure S13. Steady-State Photoluminescence Spectra for N719 dye drop-casted on glass substrate (magenta line), ZnO PNP (black line), ZnO NR (blue line) and ZnO cage (red line), films sensitized with N719 dye on glass substrates. Excitation wavelength for all the samples is 535 nm.

In order to understand the electronic interactions between N719 dye and as synthesized ZnO heterostructures (i.e., ZnO cage, ZnO PNP and ZnO NR), steady state photoluminescence (PL) analysis is performed for all the photoanodes and N719 dye drop-casted on glass substrate. Figure S11 is depicting normalized PL spectra for all the samples; namely, N719 dye (magenta line), ZnO PNP (black line), ZnO NR (blue line) and ZnO cage (red line). From Figure S11, we have observed significant quenching of PL emission intensity (indicated by olive arrow) originating from the N719 dye, when it is anchored to the ZnO. This observation infers excited state electronic interaction between N719 dye and ZnO which confirms the photoinduced charge injection from the dye molecules to the conduction band (CB) of ZnO.[2] Decreasing trend in emission intensity for the N719 dye sensitized photoanodes is ZnO PNP > ZnO NR > ZnO Cage. This is indicative of faster and efficient charge injection from the dye molecules to the ZnO cages as compared to the ZnO PNP and ZnO NRs. This can be attributed to strong electronic interaction between ZnO cage and N719 dye molecules in the photoanode.

Table S5. An overview of the present scenario of ZnO Based N719 dye sensitized solar cells and their relevant performance parameters along with photovoltaics discussed in our manuscript

Ref No.	ZnO Nanostructures	J_{sc} (mA/cm^2)	V_{oc} (mV)	*FF* (%)	η (%)	Active Area (cm^2)
SI 2	ZnO NTs	5.9	710	38	1.5	0.20
SI 3	ZnO NWs	9.3	670	34	2.1	0.50
SI 4	ZnO hierarchical NWs	8.8	680	53	2.6	No data
SI 5	ZnO mesoporous film	11.8	650	52	4.0	0.5
SI 6	ZnO self-assembled nanostructures	10.7	710	62	4.7	3.2
SI 7	ZnO nanosheet/nanowires	10.9	680	65	4.8	0.64
SI 8	ZnO NPs + scattering hollow cavities	15.7	563	62	5.5	0.20
SI 9	ZnO teterapods	16.3	656	59	6.3	0.25
SI 10	ZnO commercial nanopowder	18.1	621	58	6.6	0.25
SI 11	ZnO NWs/TiO_2 shell	15.5	770	62	7.0	0.20
SI 12	ZnO Hierarchical aggregates	19.8	640	59	7.5	0.25
Present work	**ZnO cages**	**11.8**	**720**	**50**	**4.3**	**0.25**

References:

(SI 1) J. P. Chen, L. Hong, S. Wu and L. Wang, *Langmuir*, 2002, **18**, 9413.

(SI 2) D. Barpuzary, A. S. Patra, J. V. Vaghasiya, B. G. Solanki, S. S. Soni, M. Qureshi, *ACS Appl. Mater. Interfaces,* 2014, **6**, 12629.

(SI 3) A. B. F. Martinson, J. W. Elam, J. T. Hupp, M. J. Pellin, *Nano Lett.,* 2007, **7**, 2183.

(SI 4) C. K. Xu, P. Shin, L. L. Cao, D. Gao, *J. Phys. Chem. C,* 2010, **114**, 125.

(SI 5) S. H. Ko, D. Lee, H. W. Kang, K. H. Nam, J. Y. Yeo, S. J. Hong, C. P. Grigoropoulos, H. J. Sung, *Nano Lett.* 2011, **11**, 666.

(SI 6) G. Pérez-Hernández, A. Vega-Poot, I. Pérez-Juárez, J. M. Camacho, O. Arés, V. Rejón, J. L. Peña, G. Oskam, *Sol. Energy Mater. Sol. Cells.,* 2012, **100**, 21.

(SI 7) A. Ranga Rao, V. Dutta, *Nanotechnology,* 2008, **19**, 445712.

(SI 8) F. Xu, M. Dai, Y. Lu, L. Sun, *J. Phys. Chem. C* 2010, **114**, 2776.

(SI 9) X. Sheng, Y. Zhao, J. Zhai, L. Jiang, D. Zhu, *Appl. Phys. A: Mater. Sci. Process.* 2007, **87**, 715.

(SI 10) W. Chen, Y. Qiu, Y. Zhong, K. S. Wong, S. Yang, *J. Phys. Chem. A,* 2010, **114**, 3127.

(SI 11) M. Saito, S. Fujihara, *Energy Environ. Sci.,* 2008, **1**, 280.

(SI 12) C. Xu, J. Wu, U. V. Desai, D. Gao, *J. Am. Chem. Soc.*, 2011, **133**, 8122.

(SI 13) N. Memarian, I. Concina, A. Braga, S. M. Rozati, A. Vomiero, G. Sberveglieri, *Angew. Chem., Int. Ed.*, 2011, **50**, 12321.